Supplementary Materials

Table S1. A priori calibration results of HACH 2100Q field turbidimeter.

Predefined sample (NTU)	Measurement (NTU)	Bias (%)
10	9.87	−1.3
20	196	−2
100	104	4

Table S2. Summary of post-processing of all airborne missions concluded using TXDR and CampTPWD base stations (Easting-E, Northing-N, Height-H).

Date	Station(s)	Baseline (mean, km)	PDOP (RMSE)	Solution quality (%)	Positional accuracy (m, RMSE)			Forward/reverse separation (m, RMSE)		
				Q-1	E	N	H	E	N	H
3/20/2018	CampTPWD TXDR	48.2	1.83	98.5	0.017	0.022	0.047	0.011	0.007	−0.02
3/21/2018-A	CampTPWD TXDR	32.83	1.81	99.3	0.013	0.018	0.037	0.007	0.013	0.017
3/21/2018-B	CampTPWD TXDR	27.05	1.61	99.9	0.017	0.018	0.04	0.01	0.007	0.02
3/22/2018-A	TXDR	49.26	1.18	99.6	0.014	0.018	0.038	0.009	0.013	0.03
3/22/2018-B	CampTPWD TXDR	23.96	1.67	99.6	0.017	0.018	0.042	0.023	0.009	0.056
3/29/2018	TXDR	35.59	1.67	99.2	0.019	0.021	0.05	0.018	0.017	0.12
3/30/2018-A	TXDR	40.72	1.34	99.5	0.016	0.02	0.045	0.006	0.006	0.024
3/30/2018-B	TXDR	64.12	1.74	99.1	0.021	0.022	0.051	0.022	0.026	0.12
Mean		40.22	1.61	99.34	0.02	0.02	0.04	0.01	0.01	0.05

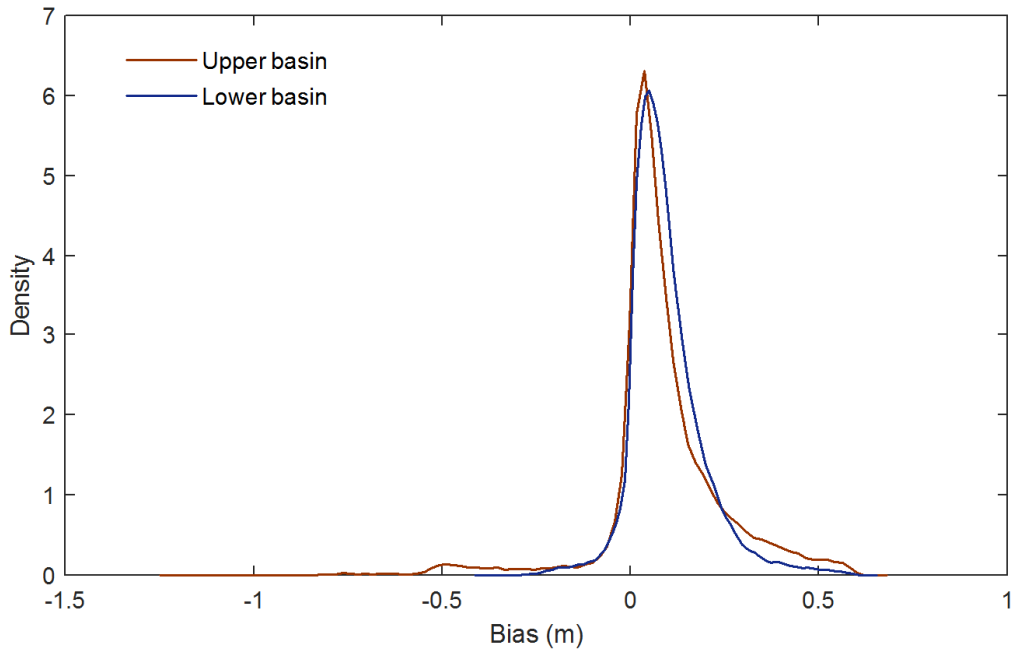

Figure S1. Distribution of Class 0 versus Class 5 for surface representation. The upper basin registered a greater sample range and worse deviation.

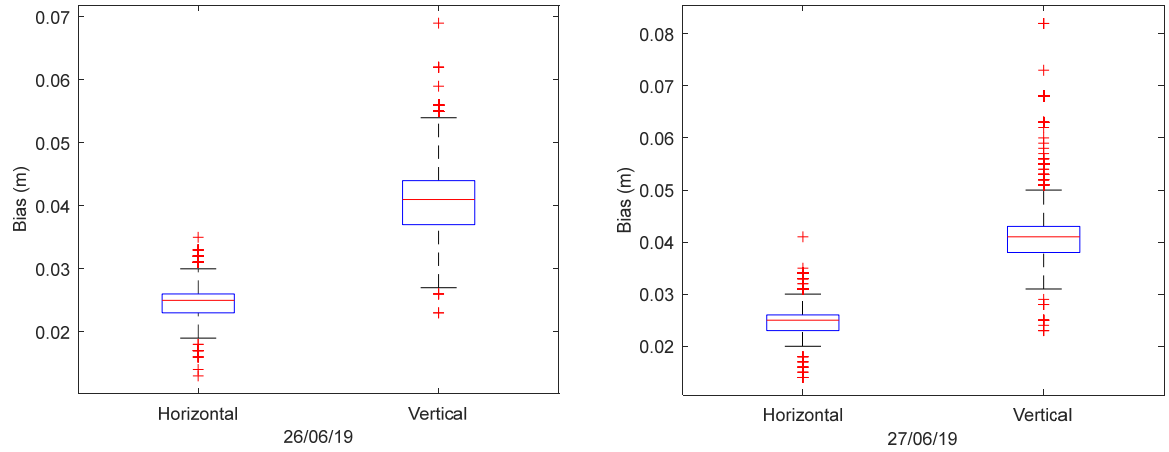

Figure S2. Median horizontal and vertical accuracy bias present in differential correction, CampTNC base station (26–27 June 2019).

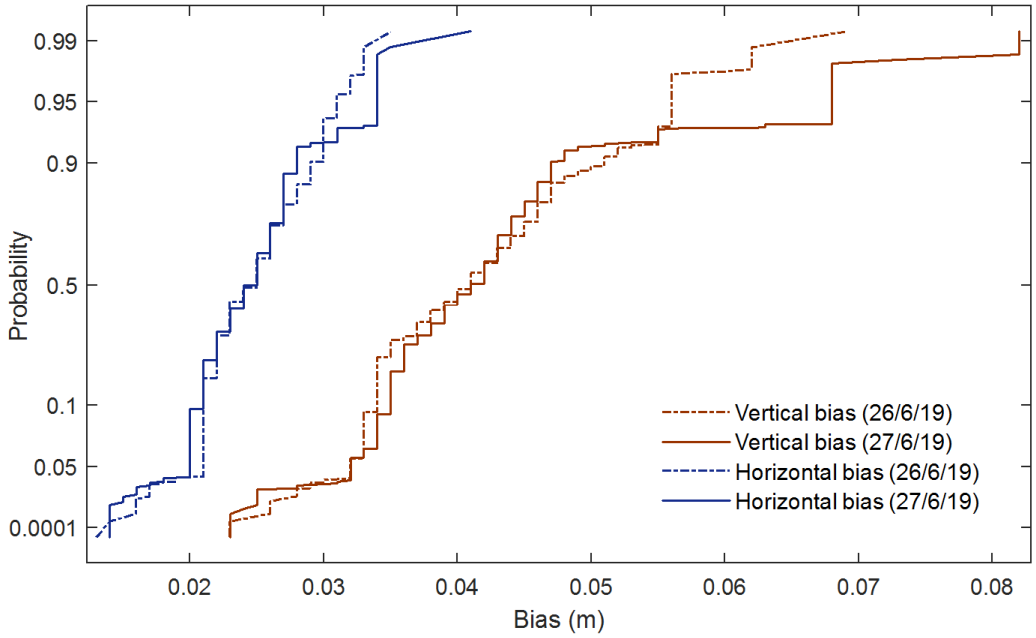

Figure S3. Probability of positional bias in differential solution applicable to localized measurements.

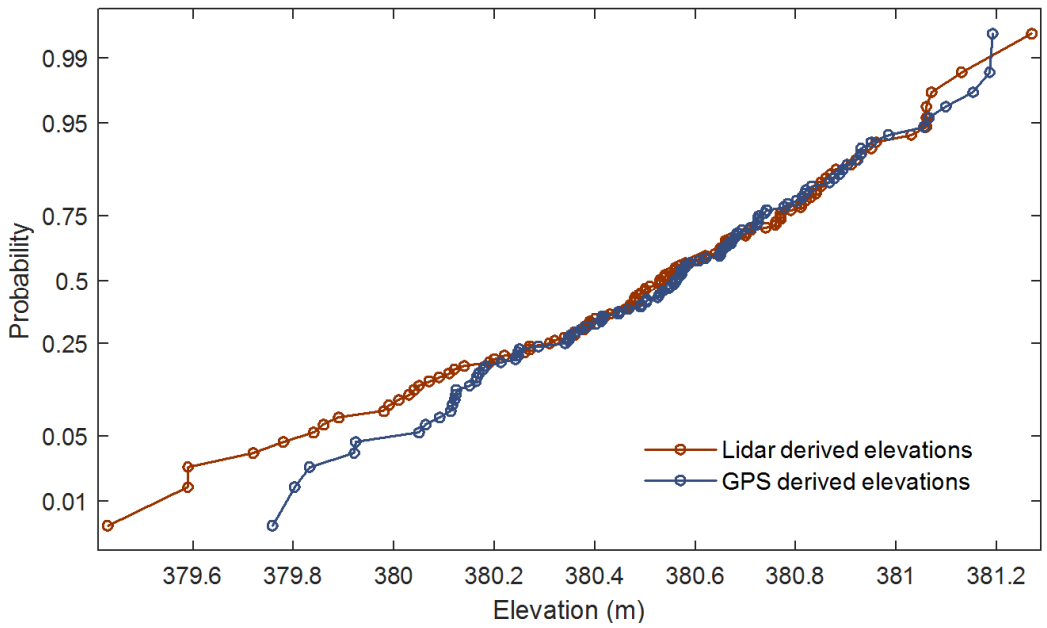

Figure S4. GPS-derived elevations indicate higher possibility of deeper measurement in the shallower areas of the river compared to Lidar-derived TIN elevations.

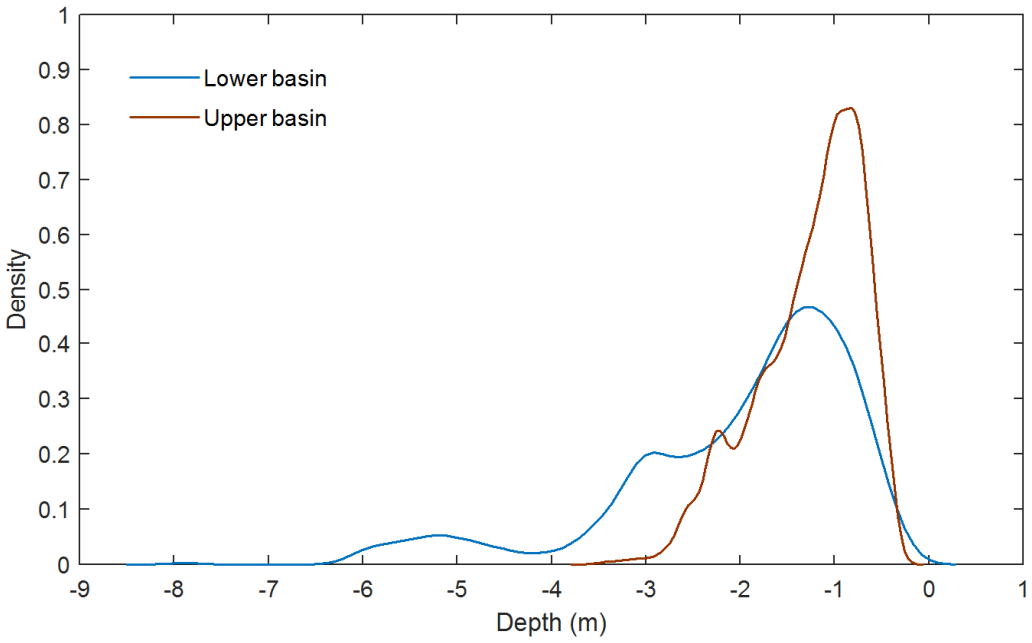

Figure S5. Density plot indicating the distribution of sonar-derived depths in the upper and lower basins surrounding Dolan Falls.